

Enhanced Raman scattering of single nanoparticles in a high- Q whispering-gallery microresonatorRui-Shan Liu,¹ Wei-Liang Jin,^{1,3} Xiao-Chong Yu,¹ Yong-Chun Liu,¹ and Yun-Feng Xiao^{1,2,*}¹*State Key Laboratory for Mesoscopic Physics and School of Physics, Peking University, Beijing 100871, People's Republic of China*²*Collaborative Innovation Center of Quantum Matter, Beijing 100871, People's Republic of China*³*Department of Electrical Engineering, Princeton University, Princeton, New Jersey 08544, USA*

(Received 27 November 2014; published 24 April 2015)

We study Raman scattering of single nanoparticles coupled to a high- Q whispering-gallery microresonator. It is found that cavity resonances greatly enhance the Raman signal, and the enhancement factor is as high as 10^8 . Unlike the noncavity case, the signal power exhibits a nonmonotonic dependence on particle size, and it reaches the maximum when the Rayleigh scattering loss and the cavity intrinsic loss are comparable. We further analyze how the Raman signal intensity is influenced by different parameters including cavity quality factors and taper-cavity coupling strength. The detection limit of observing single-nanoparticle Raman signal is discussed finally. As a potential application, this mechanism may provide an alternative way to detect specific biological targets without the need of precovered biorecognitions.

DOI: [10.1103/PhysRevA.91.043836](https://doi.org/10.1103/PhysRevA.91.043836)

PACS number(s): 42.81.Pa, 73.20.Mf, 07.60.Vg

I. INTRODUCTION

Optical microcavities supporting whispering-gallery modes (WGMs) have attracted much attention recently because of their ultrahigh quality factors, small mode volumes, excellent scalability, and ease in fiber coupling [1,2]. Light-matter interaction is significantly enhanced in these optical systems, which enables various applications ranging from fundamental physical studies to functional photonic devices [3]. As a typical scenario, when high- Q WGMs interact with a single atom or atomlike particle, such as neutral atom, quantum dot, and nitrogen vacancy center, strong coupling and vacuum Rabi oscillations can be observed when the coherent coupling strength exceeds the dissipation rates of the system [4–10]. Moreover, when the interacting particle is purely dielectric or plasmonic, the cavity resonances are observed to be strongly modified in both mode spectrum and mode pattern even when the particle is at nanoscale [11–18]. The latter triggers intense studies in highly sensitive biosensing by using high- Q WGM microcavities. For example, single nanoparticle detection and sizing have been realized experimentally by monitoring mode shift [19–24], splitting [25–28], or broadening [24,29,30], showing a high potential in label-free optical biosensing.

In general, high- Q microcavities provide a high sensitivity in optical sensing, but they cannot identify adhered particles. To selectively detect target particles, microcavity surfaces are usually functionalized by biorecognition elements [31–35], e.g., antibodies which can capture specific antigens. However, the precovering may lower the cavity quality factor, and in a realistic application, one would expect a simple method to sense the specific particles without the need of a complex biofunctionalization process. Over the past few years, the surface-enhanced Raman scattering using microcavities was proposed and shown to have great potential in specific single molecule detection [36–39]. Also, stimulated Raman lasing in WGM microcavities has been studied [27,28,40–44]. A recent experiment [45] has shown the possibility of detecting the Raman emission of a single $1\text{-}\mu\text{m}$ -radius particle in a fiber

ring resonator. Up to now, the previous theoretical studies on the cavity-enhanced single-particle Raman scattering mainly focus on the field distribution in far field in the framework of Lorentz-Mie theory [36–38]. However, for practical applications such as single-particle Raman spectroscopy and detection, the collection of the Raman signal is more efficient by using near-field waveguides. Moreover, the Raman signal intensity would be influenced strongly by the mode properties such as quality factors and coupling condition, which requires more careful treatments considering a microcavity in a real environment.

In this paper, we investigate analytically the enhanced Raman emission of a single nanometer-scale particle in a taper-coupled WGM microcavity system, as shown in Fig. 1. The WGMs greatly enhance the Raman emission signal in two ways. On the one hand, benefiting from the ultrahigh cavity quality factors of the WGMs, the circulating pump power within the cavity is strongly enhanced due to the large energy build-up factor, which leads to the first step in Raman scattering enhancement. On the other hand, considering Raman gain linewidth of most material is relatively large [46], the scattered light can also be on resonance with cavity modes, which we define as Stokes cavity modes. The Stokes cavity modes provide the second-step enhancement. In addition to the enhancement in emission rate, the Stokes cavity modes also enable a high efficiency in Raman light collection through the efficient taper-cavity coupling.

The paper is organized as follows. In Sec. II, using the Maxwell nonlinear coupled equation [11], we develop a general theory to study the Raman emission of single nanoparticles in high- Q WGM microresonators. In Sec. III, we analyze the Raman yield which is defined as the ratio of output Raman power to input pump power for different-sized particles and in different microresonators. In Sec. IV, the detection limit to observe Raman signal of a single nanoparticle is discussed. Finally, a summary is presented.

II. THEORETICAL MODEL

In this work, we consider that both the pump and Stokes light are coupled to respective cavity modes. Using the

*yfxiao@pku.edu.cn

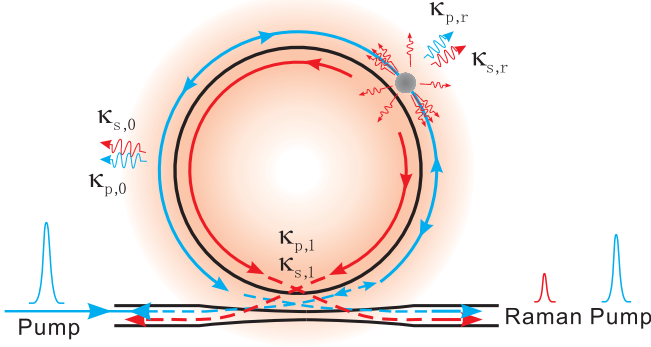


FIG. 1. (Color online) Schematic illustration of a taper-cavity system for detecting single nanoparticles, where a tapered fiber is used to excite high- Q WGMs and to collect their Raman emission. Here $\kappa_{p(s),0}$ denotes the intrinsic decay rate of pump (Stokes) cavity modes, while $\kappa_{p(s),1}$ stands for the taper-cavity coupling rate. The coefficient $\kappa_{p(s),r}$ describes the Rayleigh scattering loss by the nanoparticle itself.

Maxwell nonlinear equation and under the slowly varying envelope approximation, the rate equations of the cavity modes are [47–49]

$$\frac{da_p}{dt} = \left(i\Delta_p - \frac{\kappa_p}{2}\right)a_p - \sum_j \frac{\omega_p}{\omega_j} g_s(\omega_j) |a_j|^2 a_p - \frac{\omega_p}{\omega_s} g_s |a_s|^2 a_p + \sqrt{\kappa_{p,1}} a_{p,\text{in}}, \quad (1)$$

$$\frac{da_s}{dt} = -\frac{\kappa_s}{2} a_s + g_s |a_p|^2 a_s, \quad (2)$$

where we use the subscript “ p ” to stand for the pump cavity mode, while “ s ” stands for the Stokes cavity mode for clarity. Here $a_{p(s)}$ is the slowly varying field amplitude of the pump (Stokes) cavity mode, $a_{p,\text{in}}$ stands for the input pump wave, $\omega_{p(s)}$ is the angular frequency, and Δ_p denotes the detuning between pump light and corresponding cavity mode. The second term in Eq. (1) represents the loss from the Raman scattering into vacuum modes, where a_j , ω_j , and $g_s(\omega_j)$ are the slowly varying field amplitude, angular frequency, and Raman gain coefficient of vacuum mode j , respectively. The Raman gain coefficient of Stokes cavity mode g_s is calculated by $-6\omega_s \text{Im}(\chi_s^{(3)}) / (\epsilon_0 n_p^2 n_s^2 V_R)$ [47]. Here, $\chi_R^{(3)}$ denotes the effective third-order Raman susceptibility at the frequency shift $\omega_p - \omega_s$, and $n_{p(s)}$ is the refractive index. Since the particle radius is only tens of nanometers, we approximate the effective Raman modal volume V_R as $V_s V_p / (4f_s^2(\vec{r}) f_p^2(\vec{r}) V)$, where $V_{p(s)}$, $f_{p(s)}(\vec{r})$, and V are the cavity mode volume, the cavity-mode function, and the particle volume [47].

Note that apart from Raman emission, the particle itself also causes Rayleigh scattering which has two effects. First, it serves as a new loss channel to the optical fields with the damping rate being $\kappa_{i,r} = \alpha_i^2 \omega_i^4 f_i^2(\vec{r}) / 6\pi c^3 V_i$ ($i = p, s$), where $\alpha_i = 3V[(n_i^2 - 1)/(n_i^2 + 2)]$ is the polarizability of the particle. Second, the backscattering induces coupling between a pair of counterpropagating WGMs (i.e., the clockwise and counterclockwise cavity modes) [11]. In the case of the resolved splitting, two standing-wave modes are formed: a symmetric mode with the particle at its antinode, and

an asymmetric one with the particle at its node [25]. For symmetric standing wave, the eigenfrequency is shifted from the degenerate frequency by Rayleigh scattering, and the total damping rate is $\kappa_i = 2\kappa_{i,r} + \kappa_{i,0} + \kappa_{i,1}$ ($i = p, s$), where $\kappa_{i,0}$ and $\kappa_{i,1}$ are intrinsic cavity loss and taper-cavity coupling rate, respectively [25,30]. In comparison, the asymmetric wave mode has no mode shift from the degenerate WGM and no extra scattering loss, because the scatterer locates at its node. In this work, the referred cavity modes are actually the symmetric ones, since the asymmetric modes are not affected by the scatterer, and thus not involved in the Raman emission.

In the present work, only spontaneous Raman emission occurs. Using Eqs. (1) and (2), the threshold for stimulated Raman emission into cavity modes is derived as $P_{\text{th}} = (\kappa_s \kappa_p^2) / (4\kappa_{p,1} g_s)$. For example, at least 1 W is required to achieve stimulated emission for a 50-nm-radius particle in a cavity with intrinsic quality factor $Q_0 = 10^8$ and mode volume $V_{p(s)} = 150 \mu\text{m}^3$. Generally, owing to the small size of the nanoscale scatterers, the pump power is far below the stimulated Raman threshold for emissions into both cavity and vacuum modes. Multiplying both sides of Eq. (2) by a_s^* yields $dN_s/dt = -\kappa_s N_s + 2g_s \hbar \omega_p N_p (N_s + 1)$, where the mean cavity photon number is given by $N_{p(s)} = |a_{p(s)}|^2 / \hbar \omega_{p(s)}$. In the above equation, one supplementary Stokes photon number is added to take the spontaneous emission into account [46,48]. For spontaneous Raman emission, the mean Stokes photon number satisfies $N_s \ll 1$ (Ref. [46]). Thus we obtain the modified rate equation

$$\frac{d|a_s|^2}{dt} = -\kappa_s |a_s|^2 + G_s |a_p|^2, \quad (3)$$

where $G_s = 2g_s \hbar \omega_s$ denotes the spontaneous rate of Raman scattering.

Under the condition when both the pump and Stokes light are on resonance, using the input-output relation [50], the Raman yield Y (defined as the ratio of output Raman power P_s to input pump power P_{in}) is calculated as

$$Y = \frac{P_s}{P_{\text{in}}} = \frac{2\kappa_{s,1} \kappa_{p,1} G_s}{\kappa_s \kappa_p^2}. \quad (4)$$

To generate Eq. (4), the symmetric input mode is obtained from $|a_{p,\text{in}}|^2 = |a_{p,\text{in}}^{\text{ccw}}|^2 / 2 = P_{\text{in}} / 2$, in the absence of clockwise input. The output Stokes power is given by $P_s = \kappa_{s,1} |a_s|^2$, since both forward and backward Raman scattering can be collected by the fiber. In addition, the Raman scattering loss terms $(\omega_p / \omega_s) g_s |a_s|^2 a_p$ and $\sum_j (\omega_p / \omega_j) g_s(\omega_j) |a_j|^2 a_p$ in Eq. (1) have been neglected, as they are much smaller than other dissipations of the pump cavity mode.

III. RAMAN YIELD OF THE COUPLING SYSTEM

Throughout this paper, we approximate cavity parameters for pump and Stokes modes to be identical [e.g., $\kappa_{p,m} = \kappa_{s,m} = \kappa_m$ ($m = 0, 1, r$)], and set $\text{Im}(\chi_s^{(3)}) \sim -10^{-20} \text{m}^2 \text{V}^{-2}$, $n_{p(s)} = 1.58$, $f_{p(s)}(\vec{r}) = 0.36$, $V_{p(s)} = 150 \mu\text{m}^3$, and $\omega_{p(s)} / (2\pi) = 448(418) \text{THz}$ (Ref. [51]). Note that we use polystyrene as an example, while other materials may have larger third-order susceptibility.

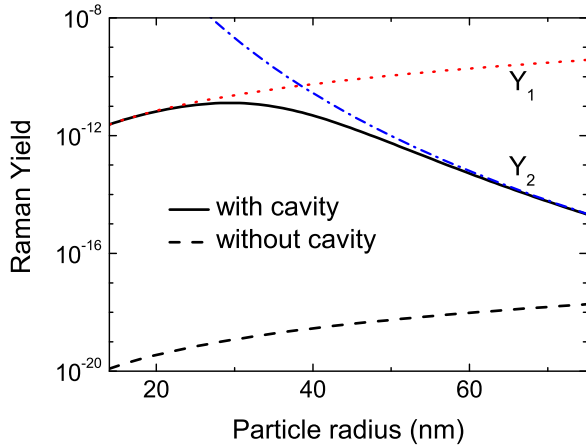


FIG. 2. (Color online) Raman yield vs particle radius in the presence (black solid) and absence (black dashed) of the cavity. The red dotted curve describes the situation when the scatterer-induced dissipation is neglected, while the blue dashed-dotted curve stands for the case when the scattering loss dominates. Here the intrinsic cavity quality factor Q_0 is set as 5×10^8 , and the system is initially at the critical coupling point ($\kappa_1 = \kappa_0$).

A. Raman scattering from different-sized particles

The solid curve in Fig. 2 presents how Raman yield depends on the particle size. The typically weak strength is owing to the inherent weakness of spontaneous Raman emission and the small size of nanoparticles. For comparison, the dashed curve in Fig. 2 also plots the Raman yield in the absence of the cavity, by assuming that the focused pump laser spot has a half wavelength in diameter.

In the noncavity case, the yield is proportional to the target volume, as expected, since the particle size determines the amount of molecules that take part in the scattering process. In the taper-cavity system, however, the dependence becomes nonmonotonic, because the particle scattering losses greatly modify the cavity field. In more detail, a large-sized particle generally causes stronger dissipation, which further reduces the pump light strength inside the cavity and weakens the Raman signal. Thus, the two size-dependent contributions, i.e., Raman gain and scattering loss, have exactly opposite effects on signal strength, and result in the nonmonotonic dependence, which will be discussed in the following. Two limits of Raman yield are considered. First, if Rayleigh scattering loss is much weaker than other dissipations, i.e., $\kappa_r \ll \kappa_0$, Eq. (4) is simplified to

$$Y_1 = \lim_{\kappa_r \ll \kappa_0} Y = \frac{2\kappa_1^2}{(\kappa_0 + \kappa_1)^3} G_s. \quad (5)$$

Note that $G_s \propto V$, which means Y_1 increases linearly with particle volume, as shown in the red dotted curve in Fig. 2. In this case, it has the same dependence as that in the noncavity case.

Second, when the particle becomes large enough and the scattering dissipation dominates cavity losses $\kappa_{p(s)} = 2\kappa_r + \kappa_0 + \kappa_1$, Raman yield is given by

$$Y_2 = \lim_{\kappa_r \gg \kappa_0} Y = \frac{\kappa_1^2}{4\kappa_r^3} G_s. \quad (6)$$

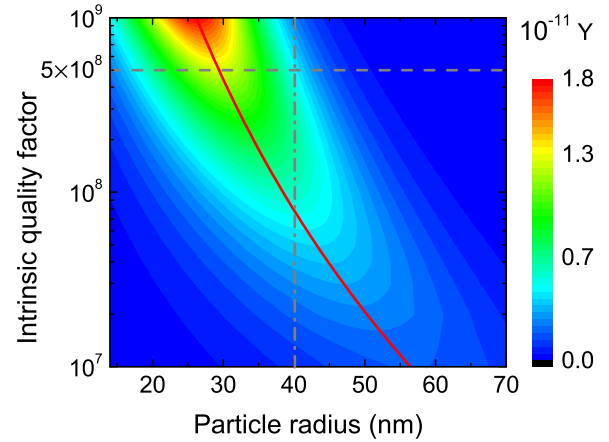


FIG. 3. (Color online) Contour plot of Raman yield as a function of particle radius and intrinsic quality factor in the case of critical coupling ($\kappa_1 = \kappa_0$). The dashed horizontal line denotes the Raman yield for different target radius when $Q_0 = 5 \times 10^8$, corresponding to the case in Fig. 2. The dash-dotted vertical line describes the yield for a given particle radius of 40 nm. The red solid curve shows the optimal κ_0 as a function of the particle radius.

With the increase of particle size, the Rayleigh scattering loss grows quickly, as the relation $\kappa_r \propto V^2$ shows. Thus we obtain $Y_2 \propto V^{-5}$, which predicts a rapid drop of signal power in this region, as indicated by the blue dash-dotted curve in Fig. 2. As expected, the yield fits Y_1 well for small-sized particles with radius below 20 nm, while it fits Y_2 well for large-sized ones with radius greater than 60 nm, as shown in Fig. 2.

In the intermediate region, the Rayleigh scattering loss induced by the particle becomes comparable with other cavity dissipations, and most importantly, there is a trade-off between the Raman gain and the Rayleigh scattering loss. With the increase of particle size, the Rayleigh scattering loss grows much faster than the Raman gain because of $G_s(\kappa_s) \propto V(V^2)$. At a critical particle size, the Raman yield reaches its maximum. Deriving from Eq. (4), when strongest Raman signal is generated, the particle radius is proportional to $Q_0^{-1/6}$, where Q_0 stands for the cavity intrinsic quality factor. The maximum yield is about 1.3×10^{-11} when the particle radius is about 30 nm in Fig. 2, which shows an enhancement factor exceeding 10^8 compared to the noncavity case. It is found that the maximum mean Stokes photon number N_s is 9×10^{-3} with an excitation power of 1 mW, which further verifies no stimulated scattering.

B. Raman yield in different microresonators

We further study the Raman yield of a single nanoparticle in different microcavities. Note that the Raman signal strength remains monotonic with regard to the cavity mode volume. Thus, Fig. 3 plots how the yield Y relies on both the target size and the cavity intrinsic quality factor Q_0 when the system is initially under the critical coupling condition. It shows the nonmonotonic dependence of signal power on particle size for a given intrinsic quality factor Q_0 . For instance, given $Q_0 = 5 \times 10^8$, the dashed horizontal line exactly corresponds to the case in Fig. 2. In principal, a higher Q_0 is beneficial

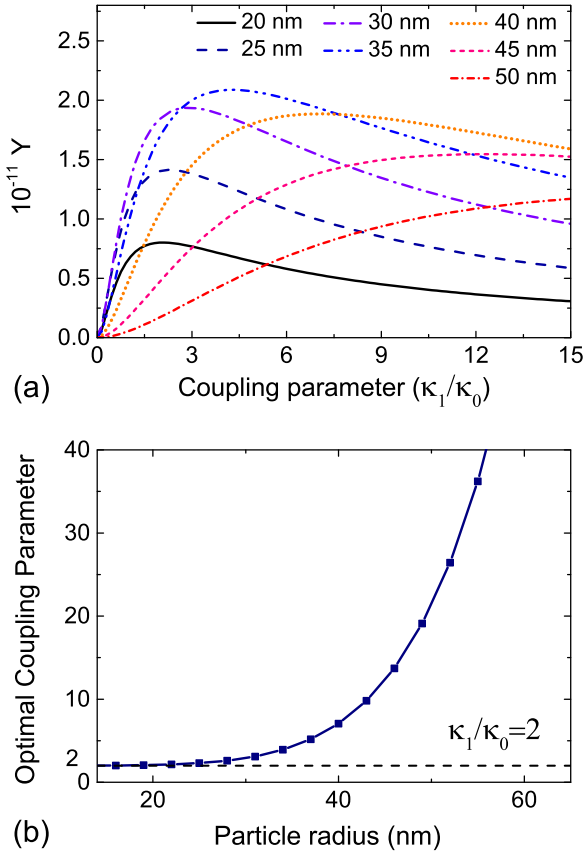


FIG. 4. (Color online) (a) Raman light yield as a function of coupling parameter κ_1/κ_0 , for different-sized particles. (b) Optimal coupling parameter for certain-sized targets. Here the intrinsic quality factor is set as 5×10^8 .

for generating a stronger Raman signal. For a given particle size (e.g., 40 nm in radius, shown by the dash-dotted vertical line), however, Fig. 3 illustrates a nonmonotonic dependence of Raman yield on Q_0 . The solid curve depicts the optimal intrinsic quality factor for a given-sized nanoparticle. The interpretation is discussed in detail in the following.

The taper-cavity coupling condition also plays an important role in both enhancing and collecting Raman emission. Different from many cases where the maximum circulating power inside a cavity is obtained when $\kappa_1/\kappa_0 = 1$, we find that the strongest Raman signal in the present study is generated when the system initially works in the overcoupling regime (i.e., $\kappa_1 > \kappa_0$). This can be understood by the two facts. First, the Rayleigh scattering loss of nanoparticles in an ultrahigh- Q microcavity is significant and it contributes to the total cavity loss just like the cavity intrinsic loss. In other words, the critical coupling condition is modified as $\kappa_1/(\kappa_0 + \kappa_r) = 1$. Second, even if the Rayleigh scattering loss can be neglected, the maximum Raman yield is achieved when $\kappa_1/\kappa_0 = 2$, instead of $\kappa_1/\kappa_0 = 1$, because both pump and Stokes cavity modes are involved.

In Fig. 4(a), we present Raman yield depending on coupling coefficient κ_1/κ_0 for different particle sizes. When κ_1/κ_0 is small, the taper cannot couple the excitation light into the cavity and collect its emission effectively, resulting in a weak signal. When κ_1 increases, we obtain a higher coupling

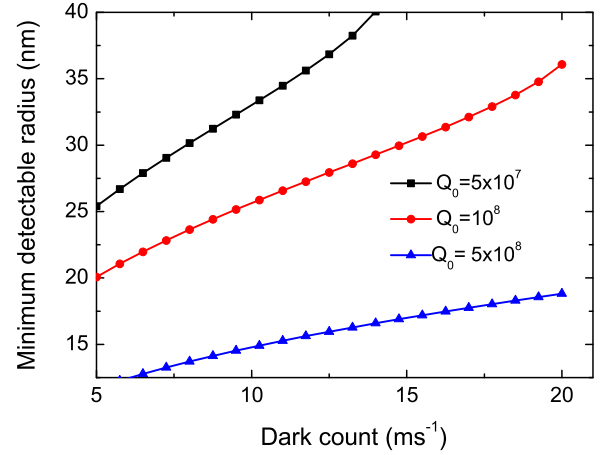


FIG. 5. (Color online) Minimum particle radius required to observe Raman light by detectors with different dark count. Cavity intrinsic quality factors are 5×10^7 , 10^8 , and 5×10^8 .

efficiency, but the total dissipation grows at the same time. The trade-off between them leads to the optimal coupling parameter value for the strongest Raman signal. For instance, the optimal coupling parameters are about 2.1, 2.8, 6.2, and 17.9, for particles with radius of 20, 30, 40, and 50 nm. The optimal coupling parameter value increases with the growth of particle size, as demonstrated in Fig. 4(b). With the increase of particle size, a larger κ_1 is demanded to compensate for the growing Rayleigh scattering loss, and the system operates most efficiently in the overcoupling region with κ_1/κ_0 exceeding 2. In addition, we emphasize that a higher quality factor always generates a stronger Raman signal, as long as the coupling parameter is adjustable.

IV. DETECTION LIMIT AND DISCUSSION

We now study the detection limit to observe the Raman signal of a single nanoparticle. In most cases, the information of targets is retrieved from the line shape of the transmission spectrum, which makes it sensitive to the noise from pump laser and thermorefractive fluctuations [52–55]. However, in our case, the Raman light frequency and intensity are our concern and the Raman signal has a frequency shift from the pump light, which makes it immune to the pump laser and thermorefractive fluctuations. The Raman signal can be detected when the transmitted Stokes photon number exceeds the value that a photodetector can distinguish [56].

Figure 5 depicts how the minimum detectable particle radius depends on the dark count rate of photodetectors. As demonstrated in the previous discussion, a higher cavity intrinsic quality factor Q_0 leads to more Stokes photons, which further predicts a lower detection limit. For example, when the dark count rate of the photodetector is 10 ms^{-1} , the Raman light from a 15-nm-radius particle is detectable for Q_0 being 5×10^8 , while for Q_0 being 5×10^7 , the minimum detectable particle is about 33 nm in radius. For comparison, the lower particle radius limit of mode splitting is calculated as 14 nm for cavities with an intrinsic quality factor of 10^8 (Ref. [25]), because the mode splitting of a passive cavity can only be resolved when the amount of splitting exceeds the total cavity

decay rate. It should be noted that we have not considered the collection efficiency of photodetectors or other detection noise, which require further studies.

The previous discussion is limited to the ideal situation when both pump and Raman light are strictly on resonance. In practice, the frequency shift of Stokes cavity mode $\Delta\omega = \omega_p - \omega_s$ can have a deviation from Raman shift Ω_R . In this case, the Raman susceptibility is given by $\chi_R^{(3)}(\Delta\omega) = 2\Omega_R\Gamma_R\xi_R/(\Omega_R^2 - \Delta\omega^2 + 2i\Gamma_R\Delta\omega)$, where Γ_R is the Raman resonance half width, and ξ_R denotes the peak susceptibility value when $\Delta\omega = \Omega_R$ [57]. When the pump light detuning Δ_p is also considered, the Raman yield Y' is obtained as

$$Y' = \frac{\kappa_p^2}{\kappa_p^2 + 4\Delta_p^2} \frac{4\Gamma_R^2\Omega_R\Delta\omega}{(\Omega_R^2 - \Delta\omega^2)^2 + 4\Gamma_R^2\Delta\omega^2} Y, \quad (7)$$

where the expression of Y is given by Eq. (4). At the Raman shift of 1601 cm^{-1} , the Raman resonance half width is $2\pi \times 138 \text{ GHz}$ for polystyrene [58]. Evidently, the cavity linewidth is much narrower than the Raman linewidth. Moreover, there could be tens of cavity modes within the Raman gain bandwidth. For microspheres, for instance, the spectra are dense due to the presence of high-order radial modes and degenerated azimuthal modes. On the one hand, the spontaneous Raman emission rate is not modified by the Purcell effect because of the broad Raman linewidth and rich WGM spectra [59], in contrast to the Purcell enhancement of Rayleigh scattering [60]. On the other hand, cavity modes which lie in the Raman gain bandwidth can help to estimate line shape of spontaneous Raman emission to some extent.

V. CONCLUSION

In summary, we have analyzed the Raman scattering of a nanoparticle in a taper-cavity system. The large cavity buildup of energy and the high efficiency in light collection strongly enhance the Raman emission signal. An enhancement exceeding 10^8 is found in this system, and the maximum Raman yield reaches 1.3×10^{-11} when the particle radius is only 30 nm. The nonmonotonic dependence of Raman signal power on particle size is also explained by considering the trade-off between the Raman gain and the Rayleigh scattering loss. We further investigate the influence of cavity parameters, including intrinsic quality factors and coupling parameters. In contrast to the conventional microcavity sensing methods by measuring the change of the pump cavity mode spectrum, monitoring Raman light intensity shows a relatively low detection limit. This cavity-enhanced Raman emission holds a great potential to sense specific particle targets without the need of precovered recognitions.

ACKNOWLEDGMENTS

This work was supported by 973 Program (Grant No. 2013CB328704), National Science Foundation of China (Grants No. 11474011, No. 11222440, No. 11121091, and No. 61435001), and Beijing Natural Science Foundation Program (Grant No. 4132058). R.-S.L. was supported by the National Undergraduate Innovational Experimentation Program and the National Fund for Fostering Talents of Basic Science (Grants No. J1030310 and No. J1103205). The authors would like to thank X. Chen for helpful discussions.

-
- [1] K. J. Vahala, *Nature (London)* **424**, 839 (2003).
 - [2] J. Ward and O. Benson, *Laser Photon. Rev.* **5**, 553 (2011).
 - [3] L. Maleki, V. S. Ilchenko, A. A. Savchenkov, and A. B. Matsko, in *Practical Applications of Microresonators in Optics and Photonics*, edited by A. B. Matsko (CRC, Boca Raton, 2009).
 - [4] E. Peter, P. Senellart, D. Martrou, A. Lemaitre, J. Hours, J. M. Gerard, and J. Bloch, *Phys. Rev. Lett.* **95**, 067401 (2005).
 - [5] Y.-S. Park, A. K. Cook, and H. Wang, *Nano Lett.* **6**, 2075 (2006).
 - [6] T. Aoki, B. Dayan, E. Wilcut, W. P. Bowen, A. S. Parkins, T. J. Kippenberg, K. J. Vahala, and H. J. Kimble, *Nature (London)* **443**, 671 (2006).
 - [7] N. Le Thomas, U. Woggon, and O. Schops, *Nano Lett.* **6**, 557 (2006).
 - [8] K. Srinivasan and O. Painter, *Nature (London)* **450**, 862 (2007).
 - [9] S. Schietinger, T. Schroder, and O. Benson, *Nano Lett.* **8**, 3911 (2008).
 - [10] B. Dayan, A. S. Parkins, T. Aoki, E. Ostby, K. J. Vahala, and H. J. Kimble, *Science* **319**, 1062 (2008).
 - [11] A. Mazzei, S. Göttinger, L. de S. Menezes, G. Zumofen, O. Benson, and V. Sandoghdar, *Phys. Rev. Lett.* **99**, 173603 (2007).
 - [12] L. Chantada, N. I. Nikolaev, A. L. Ivanov, P. Borri, and W. Langbein, *J. Opt. Soc. Am. B* **25**, 1312 (2008).
 - [13] J. Wiersig, *Phys. Rev. A* **84**, 063828 (2011).
 - [14] L. Deych, M. Ostrowski, and Y. Yi, *Opt. Lett.* **36**, 3154 (2011).
 - [15] Y.-C. Liu, Y.-F. Xiao, B.-B. Li, X.-F. Jiang, Y. Li, and Q. Gong, *Phys. Rev. A* **84**, 011805(R) (2011).
 - [16] Y. Shen and J.-T. Shen, *Phys. Rev. A* **85**, 013801 (2012).
 - [17] Y.-C. Liu, Y.-F. Xiao, X.-F. Jiang, B.-B. Li, Y. Li, and Q. Gong, *Phys. Rev. A* **85**, 013843 (2012).
 - [18] Q. Li, A. A. Eftekhar, Z. Xia, and A. Adibi, *Phys. Rev. A* **88**, 033816 (2013).
 - [19] F. Vollmer, S. Arnold, and D. Keng, *Proc. Natl. Acad. Sci. USA* **105**, 20701 (2008).
 - [20] T. Lu, H. Lee, T. Chen, S. Herchak, J.-H. Kim, S. E. Fraser, R. C. Flagan, and K. Vahala, *Proc. Natl. Acad. Sci. USA* **108**, 5976 (2010).
 - [21] J. Knittel, J. D. Swaim, D. L. McAuslan, G. A. Brawley, and W. P. Bowen, *Sci. Rep.* **3**, 2974 (2013).
 - [22] J. D. Swaim, J. Knittel, and W. P. Bowen, *Appl. Phys. Lett.* **102**, 183106 (2013).
 - [23] D. Keng, X. Tan, and S. Arnold, *Appl. Phys. Lett.* **105**, 071105 (2014).
 - [24] M. D. Baaske, M. R. Foreman, and F. Vollmer, *Nat. Nanotechnol.* **9**, 933 (2014).
 - [25] J. Zhu, S. K. Ozdemir, Y.-F. Xiao, L. Li, L. He, D.-R. Chen, and L. Yang, *Nat. Photon.* **4**, 46 (2010).
 - [26] L. He, S. K. Ozdemir, J. Zhu, W. Kim, and L. Yang, *Nat. Nanotechnol.* **6**, 428 (2011).
 - [27] B.-B. Li, W. R. Clements, X.-C. Yu, K. Shi, Q. Gong, and Y.-F. Xiao, *Proc. Natl. Acad. Sci. USA* **111**, 14657 (2014).

- [28] S. K. Ozdemir, J. Zhu, X. Yang, B. Peng, H. Yilmaz, L. He, F. Monifi, S. H. Huang, and G. L. Long, and L. Yang, *Proc. Natl. Acad. Sci. USA* **111**, E3836 (2014).
- [29] L. Shao, X.-F. Jiang, X.-C. Yu, B.-B. Li, W. R. Clements, F. Vollmer, W. Wang, Y.-F. Xiao, and Q. Gong, *Adv. Mater.* **25**, 5616 (2013).
- [30] Y. Hu, L. Shao, S. Arnold, Y.-C. Liu, C.-Y. Ma, and Y.-F. Xiao, *Phys. Rev. A* **90**, 043847 (2014).
- [31] F. Vollmer and S. Arnold, *Nat. Methods* **5**, 591 (2008).
- [32] X. Fan, I. M. White, S. I. Shopova, H. Zhu, J. D. Suter, and Y. Sun, *Anal. Chim. Acta* **620**, 8 (2008).
- [33] X. Yi, Y.-F. Xiao, Y. Feng, D.-Y. Qiu, J.-Y. Fan, Y. Li, and Q. Gong, *J. Appl. Phys.* **111**, 114702 (2012).
- [34] M. Li, X. Wu, L. Liu, X. Fan, and L. Xu, *Anal. Chem.* **85**, 9328 (2013).
- [35] H. K. Hunt and A. M. Armani, *IEEE J. Sel. Top. Quantum Electron.* **20**, 6900213 (2014).
- [36] M. Kerker, D.-S. Wang, and H. Chew, *Appl. Opt.* **19**, 4159 (1980).
- [37] L. K. Ausman and G. C. Schatz, *J. Chem. Phys.* **129**, 054704 (2008).
- [38] M. S. Anderson, *Appl. Phys. Lett.* **97**, 131116 (2010).
- [39] I. M. White, J. Gohring, and X. Fan, *Opt. Express* **15**, 17433 (2007).
- [40] H. B. Lin and A. J. Campillo, *Phys. Rev. Lett.* **73**, 2440 (1994).
- [41] V. Sandoghdar, F. Treussart, J. Hare, V. Lefèvre-Seguin, J.-M. Raimond, and S. Haroche, *Phys. Rev. A* **54**, R1777(R) (1996).
- [42] Y. Wu, X. Yang, and P. T. Leung, *Opt. Lett.* **24**, 345 (1999).
- [43] S. M. Spillane, T. J. Kippenberg, and K. J. Vahala, *Nature (London)* **415**, 621 (2002).
- [44] M. V. Chistiakova and A. M. Armani, *Opt. Lett.* **37**, 4068 (2012).
- [45] P. S. Edwards, C. T. Janisch, B. Peng, J. Zhu, S. K. Ozdemir, L. Yang, and Z. Liu, *IEEE Photonics Technol. Lett.* **26**, 2093 (2014).
- [46] R. W. Boyd, *Nonlinear Optics* (Academic, New York, 1992).
- [47] X. Yang and C. W. Wong, *Opt. Express* **15**, 4763 (2007).
- [48] X. Checoury, Z. Han, M. El Kurdi, and P. Boucaud, *Phys. Rev. A* **81**, 033832 (2010).
- [49] T. J. Kippenberg, S. A. Spillane, B. Min, and K. J. Vahala, *IEEE J. Sel. Top. Quantum Electron.* **10**, 1219 (2004).
- [50] C. W. Gardiner and P. Zoller, *Quantum Noise*, 3rd ed. (Springer, Berlin, 2004).
- [51] J. S. Kanger, C. Otto, and J. Greve, *Opt. Lett.* **20**, 2231 (1995).
- [52] M. L. Gorodetsky and I. S. Grudinin, *J. Opt. Soc. Am. B* **21**, 697 (2004).
- [53] A. B. Matsko, A. A. Savchenkov, N. Yu, and L. Maleki, *J. Opt. Soc. Am. B* **24**, 1324 (2007).
- [54] J. D. Swaim, J. Knittel, and W. P. Bowen, *Appl. Phys. Lett.* **99**, 243109 (2011).
- [55] M. R. Foreman, W.-L. Jin, and F. Vollmer, *Opt. Express* **22**, 5491 (2014).
- [56] M. D. Eisaman, J. Fan, A. Migdall, and S. V. Polyakov, *Rev. Sci. Instrum.* **82**, 071101 (2011).
- [57] D. Dimitropoulos, V. Raghunathan, R. Claps, and B. Jalali, *Opt. Express* **12**, 149 (2004).
- [58] J.-X. Cheng, A. Volkmer, L. D. Book, and X. S. Xie, *J. Phys. Chem. B* **105**, 1277 (2001).
- [59] H. Yokoyama and S. D. Brorson, *J. Appl. Phys.* **66**, 4801 (1989).
- [60] T. J. Kippenberg, A. L. Tchebotareva, J. Kalkman, A. Polman, and K. J. Vahala, *Phys. Rev. Lett.* **103**, 027406 (2009).